BBA - Bioenergetics 1860 (2019) 439–451

Contents lists available at ScienceDirect

BBA - Bioenergetics

journal homepage: www.elsevier.com/locate/bbabio

Proton leakage across lipid bilayers: Oxygen atoms of phospholipid ester linkers align water molecules into transmembrane water wires

Marine E. Bozdaganyan[a,b], Alexey V. Lokhmatikov[a,c], Natalia Voskoboynikova[a], Dmitry A. Cherepanov[d,e], Heinz-Jürgen Steinhoff[a], Konstantin V. Shaitan[b], Armen Y. Mulkidjanian[a,c,d,*]

[a] Department of Physics, Osnabrueck University, 49069 Osnabrueck, Germany
[b] School of Biology, Lomonosov Moscow State University, Moscow 119991, Russia
[c] School of Bioengineering and Bioinformatics, Lomonosov Moscow State University, Moscow 119991, Russia
[d] A.N. Belozersky Institute of Physico-Chemical Biology, Lomonosov Moscow State University, Moscow 119991, Russia
[e] N. N. Semenov Institute of Chemical Physics, Russian Academy of Sciences, 117977 Moscow, Russia

ARTICLE INFO

Keywords:
Proton potential
Bioenergetics
Ester lipids
Ether lipids
Proton permeability
Lipid ester linkers
Mitochondria
Chemiosmotic coupling

ABSTRACT

Up to half of the cellular energy gets lost owing to membrane proton leakage. The permeability of lipid bilayers to protons is by several orders of magnitude higher than to other cations, which implies efficient proton-specific passages. The nature of these passages remains obscure. By combining experimental measurements of proton flow across phosphatidylcholine vesicles, steered molecular dynamics (MD) simulations of phosphatidylcholine bilayers and kinetic modelling, we have analyzed whether protons could pass between opposite phospholipid molecules when they sporadically converge. The MD simulations showed that each time, when the phosphorus atoms of the two phosphatidylcholine molecules got closer than 1.6 nm, the eight oxygen atoms of their ester linkages could form a transmembrane 'oxygen passage' along which several water molecules aligned into a water wire. Proton permeability along such water wires would be limited by rearrangement of oxygen atoms, which could explain the experimentally shown independence of the proton permeability of pH, H_2O/D_2O substitution, and membrane dipole potential. We suggest that protons can cross lipid bilayers by moving along short, self-sustaining water wires supported by oxygen atoms of lipid ester linkages.

1. Introduction

1.1. Properties of proton flow across lipid bilayer

In humans, up to half of the cellular energy gets lost because of proton leaks through mitochondrial membranes [1,2]. In membranes of mitochondria, as well as in other energy-converting membranes, diverse enzyme complexes generate the electrochemical potential of protons (proton potential) over the membrane, which is then used mostly for the synthesis of ATP [3–5]. While most protons, being pushed by membrane voltage of > 200,000 V/cm, go through ATP synthases, some protons shirk and slide between lipid molecules or along lipid/protein interfaces, which leads to major energy losses. The proton leakage is so extensive because the permeability of phospholipid membranes to protons (10^{-4}–10^{-8} cm s^{-1} [6–22]) is by many orders of magnitude higher than that to other monovalent cations, cf with the permeability coefficients of 10^{-12}–10^{-14} cm s^{-1} for sodium ions [14,23]. In spite of its physiological importance, the mechanism of proton leakage through phospholipid bilayers remains obscure.

To avoid high proton leaks, some thermophilic and alkaliphilic prokaryotes store energy by means of electrochemical potential of sodium ions (sodium potential) and use sodium-translocating ATP synthases [24,25]. This sodium-dependent bioenergetics was shown to be evolutionary primal [26–28]. Apparently, primitive membranes of the first organisms could not hold the proton potential large enough to drive the ATP synthesis. Therefore, from the bioenergetics viewpoint, the evolution of biological membranes boils down to the evolution of their tightness to protons [5,28–31]. Even in modern organisms, the tightness of energy-transducing membranes to cations determines the overall efficiency of energy conversion [5,28,32].

Selectively high proton leakage implies efficient proton-specific passages not accessible to other monovalent cations. And indeed,

* Corresponding author at: Department of Physics, Osnabrueck University, 49069 Osnabrueck, Germany.
E-mail addresses: bozdaganyan@mail.bio.msu.ru (M.E. Bozdaganyan), alokhmat@uos.de (A.V. Lokhmatikov), nvoskobo@uos.de (N. Voskoboynikova), tscherepanov@gmail.com (D.A. Cherepanov), hsteinho@uos.de (H.-J. Steinhoff), k.v.shaitan@molsim.org (K.V. Shaitan), amulkid@uos.de (A.Y. Mulkidjanian).

https://doi.org/10.1016/j.bbabio.2019.03.001
Received 4 December 2018; Received in revised form 20 February 2019; Accepted 10 March 2019
Available online 20 March 2019

protons appear to penetrate the lipid bilayer by a specific mechanism. The proton permeability was shown to be almost independent of pH [7,14,18,20], in contrast to the concentration-dependent and diffusion-controlled permeation of other cations [17,33,34]. Biological membranes are characterized by high dipole potential (positive inside); therefore the permeability for monovalent anions is by factor 10^3–10^5 higher than for cations [35,36]. Partial collapsing of the dipole potential by phloretin increased the permeability for cations and decreased the permeability for anions by the same factor of about 10^3 [12,37]. The proton permeability was not affected by phloretin [12], which also indicates a specific proton translocation mechanism. In addition, proton permeability was weakly dependent on the H_2O/D_2O substitution [12], but strongly dependent on the fluidity [9] and thickness [17] of the membrane.

Transmembrane chains of water molecules (so-called water wires) — similar to those stretching through some proteins [38–40] or peptide channels such as gramicidin [41,42] — have been suggested to account for the proton leakage across lipid bilayers [7,14,43,44]. However, the proton-conducting water wires within peptide channels and proteins are *supported* (stabilized) by polar groups of amino acids [41–43]. For an *unsupported* water wire in the hydrophobic part of a lipid bilayer, the enthalpy of formation was estimated to be 108 ± 10 kJ/ mol [45], not to mention the large entropy loss upon aligning water molecules in the hydrophobic phase. The experimentally measured values of activation energy (E_a) of proton permeation were much lower, in the range of 30–70 kJ mol^{-1} [9,13,16,18], which rules out long, unsupported transbilayer water wires as proton conduits.

To explain the enigmatic independence of H_2O/D_2O substitution [12] and pH [7,14], Gutknecht suggested that the rate of proton permeation could be limited by a proton-independent reaction. He hypothesized that non-esterified (free) fatty acids, occasionally released upon spontaneous hydrolysis of ester bonds of phospholipids, could carry protons across the membrane [46]. Indeed, an eventual protonation of a fatty acid molecule yields an electrically neutral proton-carrying vehicle capable of crossing the bilayer by a 'flip-flop' mechanism. To maintain the proton flow, a fatty acid molecule, after releasing the proton, should "return back" in an anionic form; the overall rate of proton translocation would be then controlled by the return rate of anionic fatty acids [47], which is proton-independent. However, extraction of fatty acids from a phospholipid bilayer decreased the proton transfer rate only by one order of magnitude [46]. Later, it was shown that bilayers of archaeal phospholipids, in which polar heads are linked to isoprenoid tails by non-hydrolizable ether bonds, were only slightly less leaky to protons than fatty acid membranes of bacteria and eukaryotes [16,20]. The proton permeability through these membranes was also independent of pH [16,20], so that the pH-independence of proton permeability could not be attributed to the kinetic limitation by translocation of anionic fatty acids.

A rate limitation by a proton-independent reaction was also invoked in the "cluster contact" model of Haines [48]. This model suggested that proton can jump between the lipid leaflets when two water clusters with opposite electric charges meet in the midplane of the bilayer. The rate of proton transfer would be then determined by the probability of such encounter, which could explain both the independence of proton leakage of pH and its strong dependence on temperature and thickness of the membrane. Voth and colleagues, by using the multistate empirical valence bond (MS-EVB) approach, modelled the behaviour of protonated water clusters in the hydrophobic part of the membrane and claimed that such clusters could survive for hundreds of picoseconds [49]. They discussed their data in the context of the "cluster contact" model.

The "cluster contact" model [48], albeit highly insightful, appears to be kinetically implausible. The pK value of the H_3O^+/H_2O pair in water is −1.7. In the hydrophobic membrane phase, this value would decrease by 2–3 pH units because of desolvation penalty (for its quantitative estimates see Results below and [50]). Accordingly, the pK value of the couple H_2O/OH^-, which is +15.5 in water, would increase by the same 2–3 pH units in a hydrophobic environment. The probability that a positively charged, protonated water cluster (with $pK \ll -1.7$) would meet, in the hydrophobic midplane of a bilayer, with a negatively charged, deprotonated water cluster (with $pK \gg 15.5$) is vanishingly small. Furthermore, Voth and colleagues, in their recent paper [51], have admitted that the long life time of membrane-embedded protonated water clusters in their earlier calculations [49] was due to the introduced ban on the interaction of protons with groups other than water. When such interactions were permitted, "the protonatable sites of the lipids solvated the hydrated excess proton" (quoted from [51]). This finding discounts the earlier claims of long-living protonated water clusters in the membrane [49,52]. Therefore, the cluster contact mechanism is unlikely to support high proton permeabilities, as measured e.g. with phospholipid vesicles [7–21].

Hence, despite a plethora of experimental data [6–21] and many insightful ideas [7,14,18,22,41,43,44,46,48,53–55], the cause of high permeability of lipid bilayers to protons remains obscure.

1.2. Hypothesis: Phospholipid-mediated proton permeation

Here, in a search for a proton-independent reaction that could limit the membrane proton permeability, we explore a scenario where protons could cross the membrane by going between the phosphate groups of sporadically converging phospholipid molecules. The volume concentration of phosphate groups in the membrane is about 1 M, and their estimated pK values in the bilayer are in the range of 3.0–4.0 [13,56]. Hence, because of their higher pKa value, phosphate groups of lipids, as proton acceptors, are superior to water molecules. The involvement of phospholipids in proton transfer was proposed by DeCoursey, who suggested that phosphate groups may become protonated neutralizing their charge, so that lipid molecule could flip-flop across the membrane, releasing the proton on the other side [22]. Indeed, the estimated pK_a values of lipid phosphate groups in the membrane are comparable with those of fatty acids, which are apt proton carriers [46,47]. Being connected with the bulk solution by polar "bulges" of water molecules [52,57], these phosphate groups are in a fast proton equilibrium with the bulk [51,58]. An interaction of a proton with a negatively charged phosphate group would yield a neutral (or a quasi-neutral) moiety [51,59,60], which, as a whole, could enter the hydrophobic membrane layer. The sinking into the bilayer would increase the effective pK_a value of a lipid phosphate group owing to solvation penalty [35,50], so that the group could stay protonated. In such a case, the proton would enter the hydrophobic phase as an electrically neutral phosphate moiety, similarly to a protonated fatty acid. Still, an efficient proton transfer by flip-flopping of phospholipid molecules is unlikely. In contrast to fatty acids, phospholipid molecules, because of their bulky polar heads, cannot easily cross the membrane. Their flip-flops take many hours, so that flip-flopping phospholipids cannot sustain the observable rates of transmembrane proton transfer. Nonetheless, a protonated lipid phosphate group may move sufficiently close to an anionic lipid phosphate group from the opposing leaflet and exchange a proton, for example, via a short water wire. Proton transfer would be then limited by the rate of bringing the phosphate groups of two phospholipid molecules closer to each other. In this case, the proton transfer may proceed with lower activation enthalpy than a genuine flip-flop of phospholipid molecules (E_a > 100 kJ/ mol [61]). Being constrained by mobility of phospholipid molecules, this type of proton permeability could be independent of pH, but should depend on temperature and lipid dynamics.

To test this scenario, we combined (i) experimental measurements of proton flow across phosphatidylcholine vesicles, (ii) steered molecular dynamics (MD) simulations of phosphatidylcholine membranes and (iii) kinetic modelling. Our analysis shows that protons can go between the phosphate groups of apposing lipids via short water chains supported by oxygen atoms of lipid ester linkages. The properties of

Table 1
The list of performed MD simulations.

System #	Type of run	Trajectory length, ns	Velocity, 10^{-3} nm/ns		Distance between the two constrained groups, nm
			PO[PH]C	PO[P^-]C	
A	Equilibrium MD	100	–	–	–
B, C	Productive MD	200, 500	–	–	–
D	PMF calculation	900	1.0	2.0	Varied
E	PMF calculation	900	2.0	1.0	Varied
F, G, H	PMF calculation	600 × 3	2.5	2.5	Varied
I	PMF calculation	500	5.0	5.0	Varied
J	PMF calculation	900	2.0	2.5	Varied
K	PMF calculation	600	5.0	2.5	Varied
L	Constrained MD	200	–	–	0.95
M	Constrained MD	200	–	–	1.05
N	Constrained MD	200	–	–	1.25
O	Constrained MD	200	–	–	1.35
P, Q, R	Constrained MD	200 × 3	–	–	1.55
S, T	Constrained MD	200 × 2	–	–	1.65
U	Constrained MD	200	–	–	2.15

such proton transfer would match the experimentally determined characteristics of proton leakage through phospholipid bilayers [6–21].

2. Methods

2.1. Preparation of POPC liposomes and their characterization

Chemicals used for preparation of buffer solutions were ordered at Sigma-Aldrich (St. Louis, US) or Roth (Karlsruhe, Germany). All buffers were prepared at 40 °C, the pH-meter being calibrated accordingly. Pyranine (trisodium 8-hydroxypyrene-1,3,6-trisulfonate), valinomycin, nigericin, stocks solutions of sulfuric acid and choline chloride were derived from Sigma-Aldrich. Pure synthetic 1-palmitoyl-2-oleoyl-phosphatidylcholine (POPC) was purchased as chloroform solutions produced by Avanti Polar Lipids (Alabaster, US).

Liposomes were prepared according to Elferink et al. [62] Lipids were dried in the glass beaker under stream of nitrogen. Later on, chloroform was replaced by diethyl ether to get completely rid of organic solvent using the nitrogen flow. The lipid was hydrated with the buffer A containing 50 mM 4-morpholinepropanesulfonic acid (MOPS), pH 7.5, 75 mM KCl and 25 mM choline chloride. The suspension was several times sonicated in a water bath and the lipid was collected in a final concentration of 25 mg/ml, which corresponds to the molar concentration of approximately 33 mM. After three freeze-thawing cycles the lipids were stored at −80 °C.

Prior to the experiment, the lipids were extruded through a membrane with 200 nm pores (in a volume of 0.5–1 ml) using the Avanti Mini-Extruder, then diluted to 2.5 ml with the buffer B containing 0.5 mM MOPS, pH 7.5, 75 mM KCl and 75 mM sucrose. After that, the outer liposomal buffer was exchanged with buffer B using Sephadex G25-M column PD 10 column (Pharmacia, Uppsala, Sweden), and the suspension was finally diluted with buffer B to the final concentration of 2.5 mg/ml. Liposomes were stored on ice before the measurements.

Dynamic light scattering (DLS) measurements were performed on a Zetasizer Nano ZS (Malvern Instruments, Worcestershire, UK) at 550 nm and 25 °C. Data represent the average of three sets of 14 runs of 10 s each. The particle size distribution was obtained by using the Zetasizer software package ver. 7.02 under the assumption that liposomes were spherically shaped. A LS 55 spectrofluorimeter (Perkin Elmer, USA) was used for fluorescence measurements. The measurements were performed at excitation and emission wavelengths of pyranine at 450 and 508 nm, respectively. After each addition the suspension was briefly mixed with a glass stick.

2.2. Molecular dynamics simulations

2.2.1. System description

We used the Gromacs program, version 4.5 [63] and a NPT ensemble with semiisotropic pressure coupling (Parrinnelo-Rahman barostat [64], time constant 2 ps). The temperature was set at 313 K (Nosée-Hoover thermostat [65,66], time constant 2 ps). Lipid and water molecules were coupled independently to the heat bath. Periodic boundary conditions were applied in all three dimensions. All bond lengths were kept constant using LINCS algorithm [67]. The time step was 5 fs due to the use of heavy hydrogen atoms, the simulation time was up to 1 microsecond. Long-range electrostatic interactions were treated with the PME algorithm [68] (real space cutoff 1 nm, FFT grid spacing 0.18 nm). The Lennard-Jones potentials were computed by using a cutoff length of 1.2 nm.

The simulation system contained 100 POPC molecules and 5429 water molecules. The box size was 5.8 × 5.7 × 8.6 nm, the membrane plane was perpendicular to the z-axis. The membrane was constructed using the CHARMM-GUI interface [69] in 0,1 M KCl. One of the lipid phosphate group was protonated, it is denoted further as PO[PH]C. We used the CHARMM36 [70] all-atom forcefield with improved parameters for lipids and the TIP3P water model [71]. The system was equilibrated for 100 ns, then the production MD simulation were performed, see Table 1. We calculated the potential of mean force (PMF) for two opposed lipid molecules; one of them had a protonated phosphate group (PO[PH]C), whereas the other lipid had an anionic phosphate group (PO[P^-]C). The implementation of the PMF method is specified below. The MD simulations were carried out on supercomputers “Chebyshev” and “Lomonosov” of the Lomonosov Moscow State University.

The list of all performed simulations is given in Table 1.

The simulations could be divided into four groups:

1) Equilibrium MD simulations – equilibrium MD with no constraints, equilibration of the system (trajectory *A* in Table 1);
2) Productive MD simulations – equilibrium MD with no constraints (trajectories *B, C* in Table 1);
3) MD simulations to obtain the PMF profiles – non-equilibrium umbrella sampling MD simulations, where two POPC molecules were pulled together with different velocities (trajectories *D* - *L* in Table 1);
4) Constrained MD simulations – two phosphorus atoms were constrained in three dimensions at different R_{PP} distances (trajectories *M* - *V* in Table 1). The initial structures were taken from the MD simulation *E*, see Table 1.

2.2.2. Calculation of the potential of mean force (PMF)

The PMF profiles were calculated using the umbrella sampling method [72,73]. Harmonic potentials with the force constant of 2000 kJ/ mol nm^{-2} were applied to the phosphorus atoms of two selected lipids at opposite sides of bilayer, the reference points were moved towards each other along the *z*-axis at a constant velocity *v*, $z(t) = z_0 + vt$, where z_0 is the reference position relative the membrane center. Additional position restraints were applied to fix the moving lipids in the *xy*-plane. The PMF was calculated as an integral of the averaged applied force. Variation of the pulling velocities in the range of 1–20 nm/μs changed the magnitude of PMF in the middle of membrane not more than by 10 kJ/mol, which indicates that perturbations of the system were adiabatic.

2.2.3. Visualization

Visualization of the MD simulation data was performed by the VMD software [74].

3. Results

3.1. Measurement of the activation enthalpy of proton permeation across phosphatidylcholine vesicles

The published E_a values for proton permeation across lipid bilayers [9,13,16,18] vary in a rather broad range from approx. 70 kJ/mol [9] to approx. 30 kJ/mol [13]. To specify the E_a value of proton permeation, we measured the proton transfer across the membranes of liposomes made of synthetic 1-*p*almitoyl-2-*o*leoyl-sn-glycero-3-*p*hosphocholine (phosphatidylcholine, POPC), i.e. exactly the same phospholipid that we used in our MD simulations.

We followed the approach pioneered by Deamer and co-workers [7,14,17]. Membrane vesicles (liposomes) were prepared according to Elferink et al. [62]. The particle size distribution, as determined by DLS, yielded an average diameter of 150 nm (Fig. S1 in Supplementary material, SM).

The liposome suspension (2 ml) was mixed with 10 μM pyranine in a cuvette and then heated to the appropriate temperature inside the cuvette holder. Then, 1.5 μM valinomycin were introduced to the system followed by acidification by 400 nmol of H^+ (4 μl 50 mM H_2SO_4), see Fig. 1a. After recording of the proton transfer kinetics by pyranine fluorescence (λ_{ex} 450 nm and λ_{em} 508 nm) for ~20 min, nigericin (1.5 μM) was added to equilibrate the proton concentration across the membrane (Fig. 1a). In addition to monitoring pH changes by pyranine fluorescence, we concurrently measured the pH level by an electrode. As next, 100 nmol of choline hydroxide and sulfuric acid were added to liposomes to check the linearity of pH changes measured using two approaches, as well as in order to calculate the total buffer capacity of the system.

Since the mean diameter of liposomes was found to be 150 nm (see Fig. S1 in the SM), the internal volume of uniform liposomes (at the lipid concentration of 2.5 mg/ml) amounted 1.6% of the total volume of the cuvette solution (V = 2 ml), the total surface of vesicles in the cuvette $S = 1.3 * 10^4$ cm^2. A typical ΔpH shift in response to the addition of Δn = 400 nmol H^+ was ~0.3 units. The outer buffer capacity estimated as β_{out} = Δn/V/ΔpH was 0.48 mM. The total buffer capacity of the system (including the liposome interior) β_{total} = 0.65 mM was determined by the three pH values, which were measured (a) before the addition of 400 nmol H^+ in the beginning of experiment, (b) after the addition of nigericin, and (c) after the final addition of 100 nmol H^+ (Fig. S1).

To determine the proton permeation of the membrane, it was necessary to measure the flow of protons through the membrane immediately after adding acid to the external volume. The kinetics of changes in fluorescence after the addition of protons noticeably deviated from the exponential law, similarly to earlier observations of Grzesiek and Dencher [13]. The deviation could be caused by several factors. Firstly, the manual mixing of the sample could distort the proton transfer dynamics in the first few seconds after the addition of protons. Secondly, the vesicles were characterized by a certain size distribution (Fig. S1), so that the proton equilibration times in particles of different radii would be different. This would result in a decay function differing from a simple exponential solution of the flux equation. Thirdly, the flux itself may be non-exponential: the dependence is linear for small pH changes ($2.3\Delta pH \ll 1$), but this condition is not completely fulfilled (ΔpH ≈ 0.3). Finally, slow pH drift (owing e.g. to a CO_2 effect) may have affected the kinetics during long-time measurements. By these reasons, the fluorescence dynamics after the 400 nmol H^+ addition was approximated by the sum of two exponential terms and one linear term:

$$F(t > 0) = F_1 \cdot \exp(-t/\tau_1) + F_2 \cdot \exp(-t/\tau_2) + \Delta F_0 + B \cdot t \quad (1)$$

here F_i and τ_i are the amplitudes and the relaxation times of two exponential components of the proton flux across the lipid membrane caused by the 400 nmol H^+ addition (the thin green curve in Fig. 1a), whereas ΔF_0 and *B* are the final fluorescence level and the slope of the pH drift in the system, respectively (the dashed red line in Fig. 1a corresponded to the fluorescence level after the addition of nigericin, see the thick red line). We fitted the kinetics by two exponentials just for convenience, without attributing physical meaning to separate kinetic components. Because the proton permeability is determined by the instantaneous amplitude of proton flux immediately after pH drop, we calculated the initial proton flux at $t = 0$ from the slope of the fitting curve by using the equation.

$$J_H = \frac{\Delta n \cdot (F_1/\tau_1 + F_2/\tau_2)}{\Delta F_0 \cdot S} \quad (2)$$

here Δn is the amount of added protons ($4 * 10^{-7}$ mol), *S* is the membrane surface area, and $F_1/\tau_1 + F_2/\tau_2$ are the slopes of pH changes after the addition of protons (the blue dashed line in Fig. 1a). The proton permeability P_H was calculated using the found flux value and the proton concentration change after the 400 nmol H^+ addition:

$$P_H = J_H/\Delta[H^+] = \frac{J_H \cdot V \cdot \beta_{out}}{2.3 \cdot \Delta n \cdot 10^{-pH}} = \frac{(F_1/\tau_1 + F_2/\tau_2) \cdot V \cdot \beta_{out}}{2.3 \cdot \Delta F_0 \cdot S \cdot 10^{-pH}} \quad (3)$$

where the proton permeability coefficient P_H relates the proton flux across the membrane J_H with the proton concentration difference between the two sides of membrane $\Delta[H^+]$. After addition of protons to the lipid vesicles exterior ($\Delta n = 4 \cdot 10^{-7}$ mol), the initial pH shift is $\Delta pH = \frac{\Delta n}{V \cdot B_o}$, where *V* is the cuvette volume and B_o is the pH-buffer capacity of the external solution. The respective initial difference of free proton concentration between two sides of membrane vesicles is

$$\Delta[H^+] = 10^{-pH}(1 - 10^{-\Delta pH}) \approx 2.3 \cdot 10^{-pH} \frac{\Delta n}{V \cdot B_o} \quad (4)$$

Combining this linear approximation with the Eq. (3) for the proton flux inside the vesicles, we could find the linear differential equation for the proton relaxation dynamics:

$$\frac{d[H^+]}{dt} = -2.3 \frac{P_H \cdot S}{V \cdot B} \cdot 10^{-pH} \cdot [H^+] \quad (5)$$

here *B* is the total buffer capacity of the system. The characteristic time of proton relaxation is

$$\tau_H = \frac{V \cdot B}{2.3 \cdot P_H \cdot S} 10^{pH} \quad (6)$$

This expression was derived previously by Grzesiek and Dencher, see Eq. (14) in ref. [13]. It is noteworthy that, while the proton permeability coefficient P_H is independent of pH, the proton relaxation time depends on pH, the total buffer capacity of the system, and the surface/volume ratio of the lipid emulsion.

The proton permeability coefficients P_H, as calculated from the data obtained at different temperatures, were approximated by the

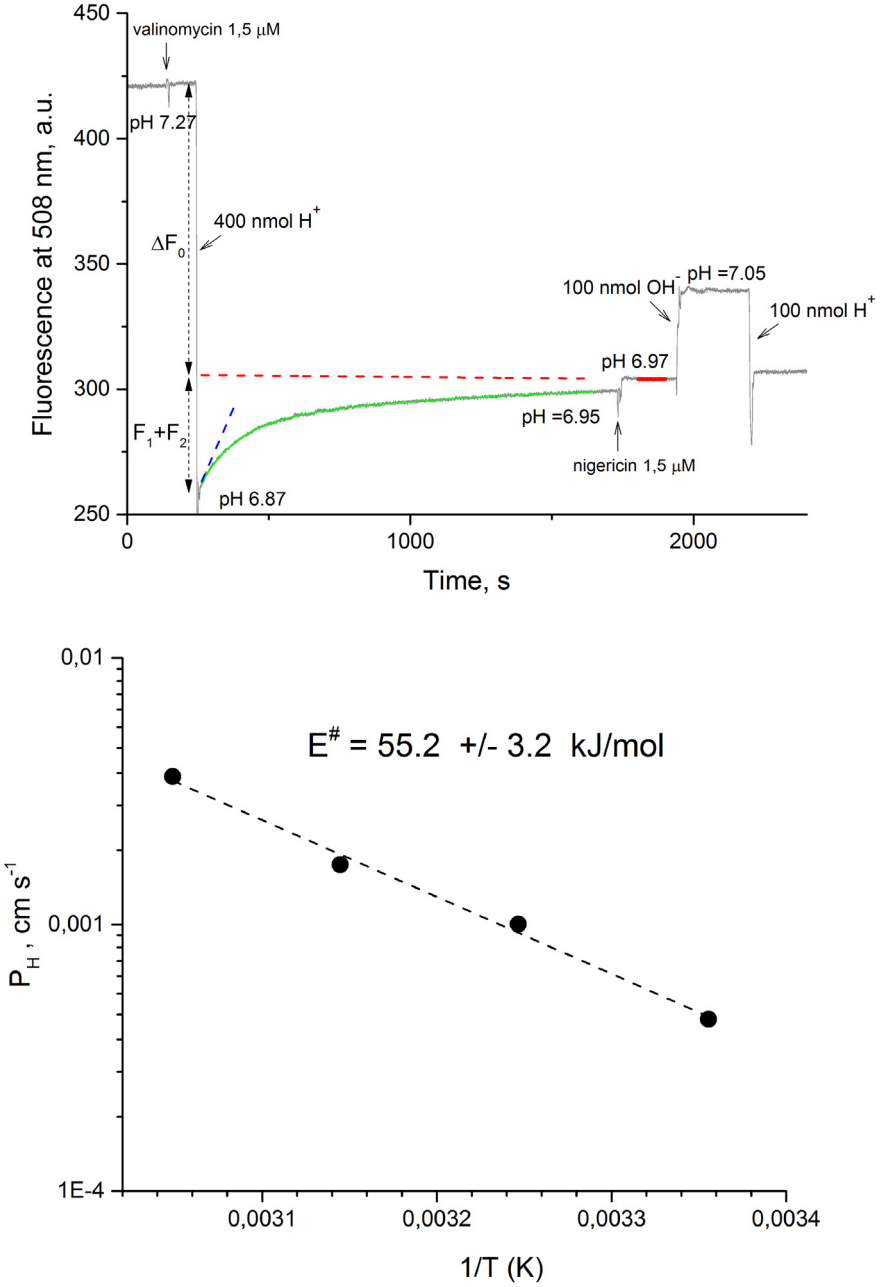

Fig. 1. Proton leakage through a POPC bilayer. a, Experimental measurements of proton flow through POPC liposomes (2.5 mg/ml) at 45 °C. The pH changes were measured by changes in pyranine (10 μM) fluorescence, while being also recorded by a pH electrode. The arrows indicate additions of 1.5 μM valinomycin, 400 nmol H^+ (as H_2SO_4), 1.5 μM nigericin, 100 nmol OH^- (choline hydroxide), 100 nmol H^+; b, Estimation of activation energy for the proton permeability measurements with pure POPC liposomes. Depicted is the Arrhenius plot for proton permeability coefficients as measured at different temperatures.

Arrhenius equation (Fig. 1b). The effective activation enthalpy $E^* \cong E_a$ could be estimated as 55.2 ± 3.2 kJ/mol (Fig. 1b). The here obtained E_a value falls within the range of previously published values of 30–70 kJ/mol [9,13,16,18].

3.2. Molecular dynamics simulations

Unlike the bulk proton flow through lipid bilayers (Fig. 1), single events of proton permeation across the midplane of the bilayer are experimentally still untraceable, so that computation remains the only option. In the first set of our molecular dynamics (MD) simulations, two molecules of POPC were slowly pulled towards each other (see Fig. 2, Table 1 in the Methods Section, Fig. S2a–g in the SM and [75] for details). By applying harmonic restraints, the phosphorus atoms of two selected lipids were moved along the reaction coordinate (z-axis) at a constant velocity. In Fig. 2a–c and Fig. S2a-g, the upper molecule (PO[PH]C) had a protonated, electrically neutral phosphate group; the phosphate group of the lower molecule was negatively charged (PO[P^-]C). As the distance between the two phosphorus atoms (R_{PP}) became ≤1.6 nm, the oxygen-rich ester moieties of the two lipids joined into a specific structure, hereafter 'oxygen passage' (see Fig. 2b). As next, a wire of seven water molecules stretched along the chain of eight oxygen atoms (Fig. 2c). We repeated the MD simulations several times and pulled the POPC molecules with different velocities, see Table 1, Fig. S2a–g in the SM and [75]. In each case, a water wire appeared.

The Fig. 3a, as well as Fig. S3 in the SM show the calculated potentials of mean force (PMF) that characterize the free energy change of lipid molecules during the motion. The PMF increased upon moving the

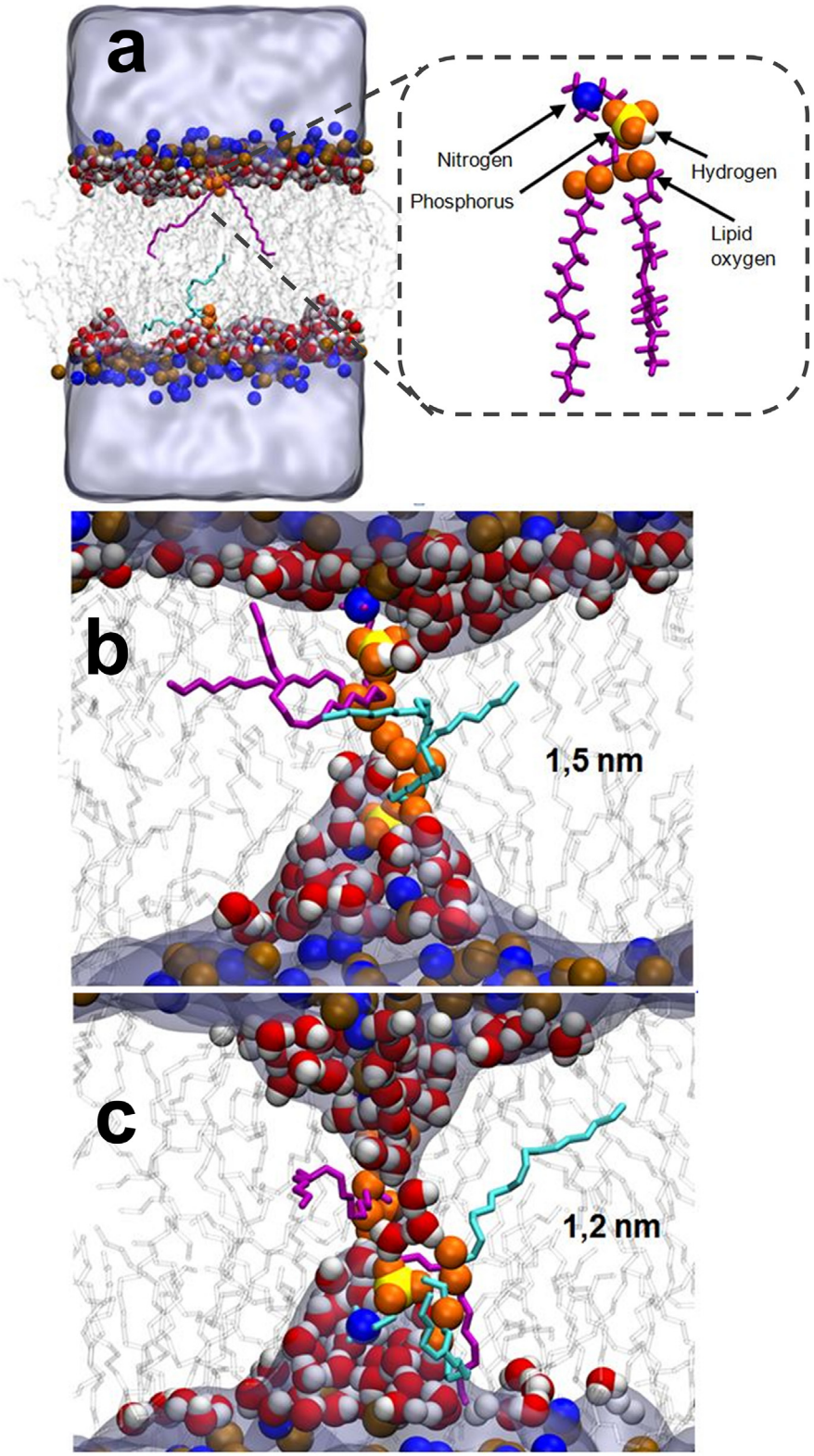

Fig. 2. Formation of a water wire upon pulling together two POPC molecu les (see also Figs. S2a–g and S3 in the Supplementary material). a, The initial system, shown after 100 ns equilibration at 313 K in 0.1 M KCl, included 100 POPC lipid molecules and 5429 water molecules. The phosphorus atoms of two lipid molecules were moved along the reaction coordinate (*z*-axis) at a constant velocity of 2.5 nm/μs (trajectory *H* in Table 1). The lipid molecules that were pulled towards each other are shown in purple (a protonated phosphate group, PO[PH]C, the total charge +1) and cyan (an anionic phosphate group, PO[P$^-$]C, the total charge zero); the tails of other lipids are shown as grey lines. In water molecules, the atoms of oxygen are colored red and atoms of hydrogen are colored white. The atoms of phosphorus and nitrogen are shown as ochre and blue van der Waals spheres, respectively, see also an all-atom model of a PO[PH]C molecule on the insert; b, Formation of an oxygen rail between two POPC molecules at the distance R_{PP} of 1.5 nm; c, Formation of a water wire at R_{PP} = 1.2 nm.

lipids towards the midplane of the bilayer. The overall PMF profiles were asymmetric relative to the midplane of the membrane (Figs. 3a, S3) because the barrier slopes for PO[P$^-$]C (left panels) were steeper than that for PO[PH]C (right panels), in agreement with the deeper position of a protonated phosphate group in the membrane (Figs. S4, S5 in the SM). The overall potential of the system as a function of the R_{PP} distance is shown in Fig. 3b.

Using the PMF profiles shown in Figs. 3 and S3, we calculated the effective pK_a value of a POPC phosphate group as a function of its position within the lipid bilayer. For this purpose, we compared the free energy profile for the charged PO[P$^-$]C (red line in Fig. 4) with that of the neutral PO[PH]C (blue line in Fig. 4). At pH 6.5, the free energy of PO[PH]C at the interface is by ~14 kJ/mol (ΔpH = 2.5) higher than that of PO[P$^-$]C (blue arrow). When PO[P$^-$]C is dragged into the

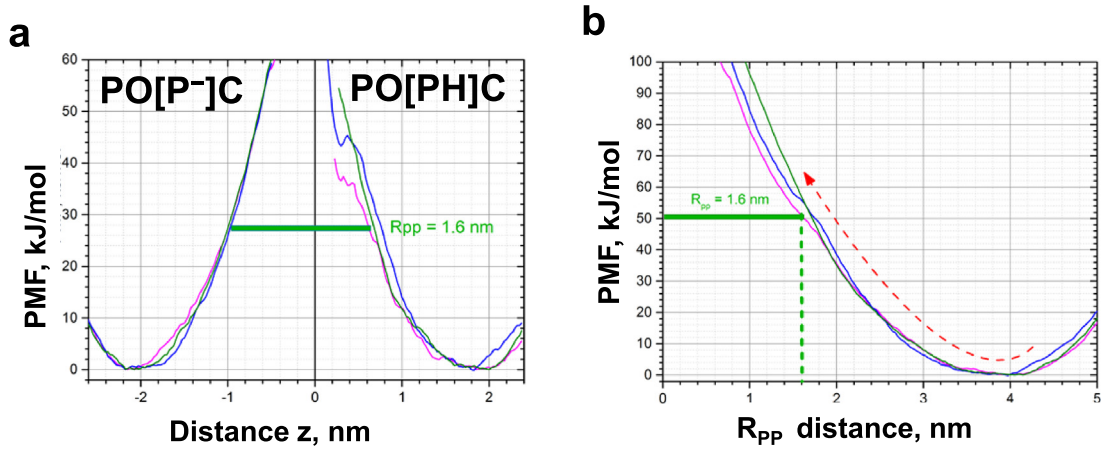

Fig. 3. Potential of mean force (PMF) for the two dragged lipid molecules as function of the distance. a, The PMF profiles for three different MD simulation runs (trajectories *F* (pink), *H* (blue) and *K* (green), respectively, in Table 1, see also Fig. S3 in the SM) with the PO[P⁻]C molecule shown left and the opposed PO[PH]C molecule shown right. The midplane of the membrane was set at zero on the *x*-axis. b, The free energy of two dragged POPC molecules as a function of the R_{PP} distance (as calculated for the three trajectories in Fig. 3a).

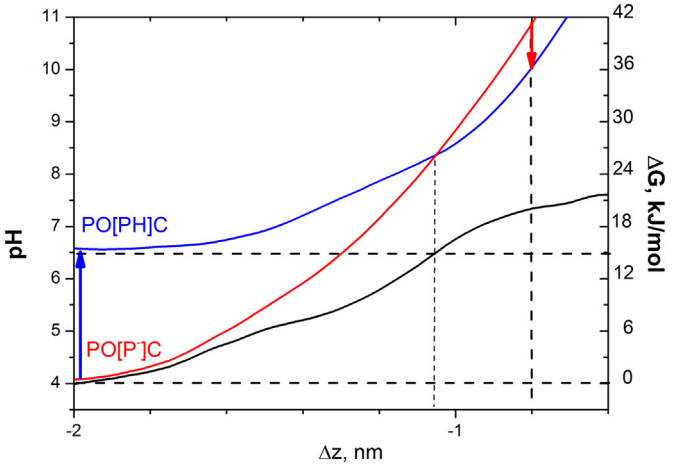

Fig. 4. Free energy profiles of PO[PH]C (blue line) and PO[P⁻]C (red line) within a lipid bilayer as a function of the distance to the midplane Δz. The effective pK_a of the phosphate group (black) was calculated assuming that its pK_a value is 4.0 at the surface of the membrane [26].

bilayer, the energy difference between the states diminishes, so that the energies of two states equalize at the distance of ~1 nm from the bilayer midplane (thin dashed vertical line).

Hence, the preconditions for proton transfer between the phosphate groups are achieved already at R_{PP} ~2 nm, i.e. even before the formation of an oxygen passage. Closer to the midplane, the free energy of PO[PH]C became lower than that of PO[P⁻]C, so that the protonated form dominates. The slopes of both curves are similar in the hydrophobic part of membrane, so that the free energy difference between states does not change further with the depth. For illustration, when the distance between two groups R_{PP} is 1.6 nm (the red arrow), the energy gap between the two states is approx. 6 kJ/mol, cf with Fig. 3.

To estimate the probability of formation of water wires and to avoid perturbations caused by pulling the lipid molecules, we performed another set of MD simulations where the PO[PH]C and PO[P⁻]C lipid molecules were hold at different, prefixed R_{PP} distances. As shown in Fig. 5a–c, the formation of oxygen passages took about 20 ns at a R_{pp} distance of 1.5 nm. After the oxygen passage had formed, the chain of water molecules promptly stretched along it (Fig. 5d, see also Table 1).

Fig. 6 shows the probability of a water wire formation as a function of the R_{pp} distance. Calculations were performed for a series of 10 trajectories, where the two phosphate groups were restrained at six different R_{PP} distances (see trajectories *M* - *V* in Table 1). Each trajectory included 10^4 frames sampled at 20 ps intervals. Each frame was analyzed for the presence of a water wire connecting the phosphate groups, and the total probability of wire formation was calculated. As it follows from Fig. 6, water wires formed rarely at $R_{PP} > 1.65$ nm; the probability of their formation increased exponentially when R_{PP} was in the range of 1.6–0.9 nm, ultimately approaching unity.

We also measured the life time of water wires after releasing the constrains. The water wires persisted for ~20 ns upon constrains removal at R_{PP} of 0.94 nm (Fig. 7).

In sum, as shown in Figs. 2, 5 and S2a–g, the water molecules lined up along the oxygen atoms of phospholipid ester linkages. In all our MD simulations (Figs. 2, 5, S2a–g, Table 1), water wires appeared after oxygen passages, which indicates that the formation of water wires was kinetically controlled by formation of the supporting polar templates.

3.3. Kinetic modelling of proton leakage through phospholipid bilayer

Drawing together two opposing lipid phosphate groups within the membrane increases the probability of the formation of a water wire (Fig. 6), but is thermodynamically costly (Figs. 3, S3). For a unit membrane area, the rate constant k_W of water wire formation could be calculated, using the free energy profiles $\Delta G(z)$ for the phosphate groups diffusion at the lipid/water interface (Fig. S5), by the equation:

$$k_W = \sigma_{POPC} \cdot \frac{\int_0^\infty \tau_D(\Delta z)^{-1} \times P_W(\Delta z) d\Delta z}{\int_0^\infty \exp(-\Delta G(z)/k_B T) d\Delta z} \quad (7)$$

here σ_{POPC} is the surface density of phosphate groups in a POPC bilayer, Δz is z-projection of the distance between two groups ($\Delta z = R_{PP} \times \cos\theta$), and $\tau_D(\Delta z)$ is the mean first-passage time of the system motion uphill the barrier:

$$\tau_D(\Delta z) = \tau_0 \times \exp(\Delta G(\Delta z)/k_B T) \quad (8)$$

where τ_0 is the characteristic time of thermal motion of a phosphate group at the lipid–water interface, $\Delta G(\Delta z)$ is the free energy barrier, and $P_W(\Delta z)$ is the probability of wire formation at the given distance between two phosphate groups. The characteristic time τ_0 could be estimated as 2 ns (see Fig. S6); it was comparable with the lifetime of the thermal motion of phosphate groups at the lipid–water interface (5 ns, Fig. S7), which is not surprising proviso that both these processes are controlled by the mobility of phospholipid molecules within the bilayer.

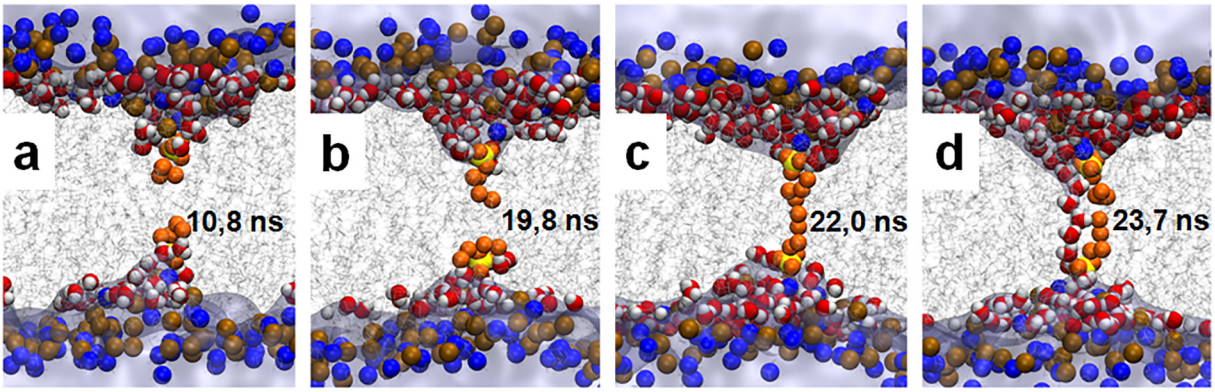

Fig. 5. Formation of a water wire between the phosphorous atoms (yellow spheres) of the two lipid molecules statically restrained at the distance R_{PP} of 1.5 nm. The time from the start of the MD simulation is indicated on the panels. a, no contact between the ester groups;
b, the ester groups start to converge; c, formation of an oxygen rail; d, a water wire aligns along the oxygen rail. Color code as in Fig. 2.

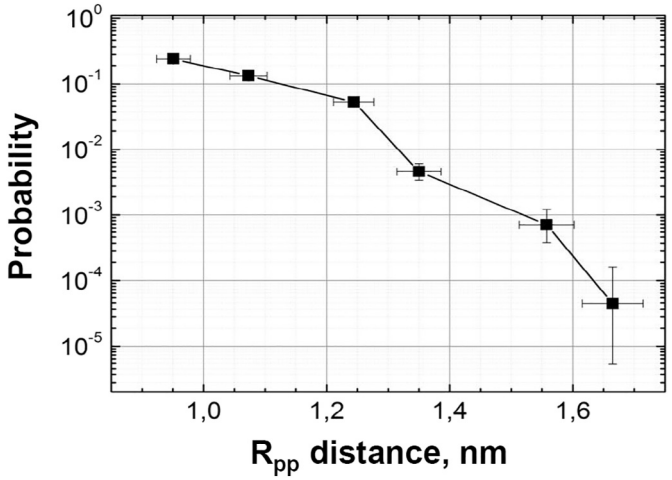

Fig. 6. The probability of a water wire formation as a function of the R_{PP} distance. The horizontal bars indicate the RMSD values of the constrained distances during the simulation; the vertical bars show the 95% confidence intervals for the probability estimates.

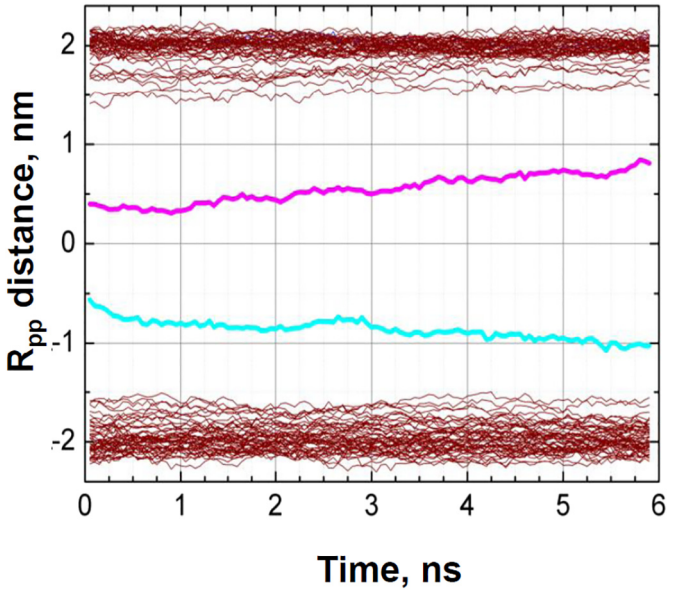

Fig. 7. Disruption of a water wire after releasing the harmonic constraints (at R_{PP} of 0.94 nm). The dynamics were averaged by 10 independent trajectories. The average positions are plotted for the protonated phosphate group of the initially constrained PO[PH]C molecule (purple), the anionic phosphate group of the opposing, initially constrained PO[P^-]C molecule (light blue) and the anionic phosphate groups of other POPC lipids in the membrane (brown).

Taking the dependence $\tau_D(\Delta G)$ from Fig. S6, the dependence $\Delta G(\Delta z)$ from Fig. 3b, the dependence $P_W(\Delta z)$ from Fig. 6, we calculated the product $\tau_D(\Delta z)^{-1} \times P_w(\Delta z)$ as a function of distance R_{PP} (see Fig. 8). We found that the optimal distance for the wire formation Δz_{opt} was ~1.6 nm. The surface density of phosphate groups in a POPC bilayer [13,56] is $\sigma_{POPC} = 1.5 \times 10^{14}\,cm^{-2}$. The numerical integration of Eq. (7) yielded the water wire formation rate $k_W = 1.26 \times 10^{11}\,cm^{-2}\,s^{-1}$.

The total rate of proton transfer as a function of the distance R_{PP} can be calculated by a similar way as the integral over its z-projection:

$$k_{PT} = \frac{\int_0^\infty \tau_D(\Delta z)^{-1} \times P_W(\Delta z) \times P_{hop}(\Delta z) d\Delta z}{\int_0^\infty \exp(-\Delta G(z)/k_B T) d\Delta z} \quad (9)$$

here $P_{hop}(\Delta z)$ is the probability of proton hop along the formed wire as a function of Δz. Water wires that stretched between two interacting phospholipid molecules (Figs. 2, 5, S2a–g) resembled the file of eight water molecules that forms after two gramicidin molecules join together to build a (transient) membrane channel [40–42,76]. In both cases, water molecules form a linear chain, which favours tight hydrogen bonds between water molecules and, accordingly, a fast proton transfer [40,77–79] by a proton-hopping mechanism, as initially suggested by Grothuss [55,80]. The overall time of the transmembrane proton translocation through a gramicidin channel is approx. 1 ns [42,81], whereby the proton transfer along the water chain per se, being determined by the mobility of water molecules, is estimated to proceed at a picosecond timescale or even faster [76–78,82]. Hence, the lifetime of water wires in our MD simulations (up to 20 ns, see Fig. 7) was long enough for an effective proton exchange ($P_{hop}(\Delta z)$ close to unity).

Taking, as previously, the dependence $\tau_D(\Delta G)$ from Fig. S6, the dependence $\Delta G(\Delta z)$ from Fig. 3b, the dependence $P_W(\Delta z)$ from Fig. 6, and assuming $P_{hop}(\Delta z)$ equals to unity, we calculated the product $\tau_D(\Delta z)^{-1} \times P_w(\Delta z) \times P_{hop}(\Delta z)$ by the same function of distance R_{PP} as shown in Fig. 8. At the optimal value of R_{PP} for proton transfer of ~1.6 nm, the numerical integration of Eq. (9) yielded the proton transfer rate $k_{PT} = 8.4 \times 10^{-4}\,s^{-1}$.

The surface concentration of protonated phosphate groups is $\sigma_{POP(H)C} = 10^{(pKa)-(pH)} \times \sigma_{POPC}$, where pKa is the functional pK_a of phosphate groups at the lipid–water interface. For POPC membranes this pK_a value could be estimated as ~4.0 [56]. Taking the surface density of phosphate groups in a POPC bilayer

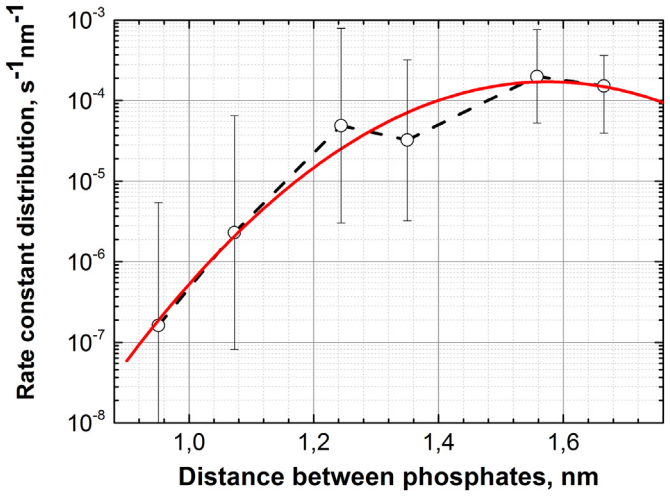

Fig. 8. Rate of water wire formation between opposing PO[PH]C and PO[P$^-$]C molecules as a function of distance R_{PP}. The points, as calculated using the data in Figs. 3b, 6, S5, and S6, were approximated by a parabola with the maximum at R_{PP} = 1.55 nm (red line). The probability of water wire formation was calculated from the MD simulations with the distance between two phosphorus atoms R_{PP} being constrained by two static parabolic potentials (Table 1, MD simulation runs *M*, *N*, *O*, *P*, *Q*, *R*, *S*, *T*, *U*, *V*). Ten representative initial configurations of the system with different R_{PP} values (see the last column in Table 1) were taken from the PMF trajectory *E*, the respectively different static parabolic potentials were imposed and the system was equilibrated for 800 ns, after which productive, constrained MD simulations were performed for 200 ns (trajectories *M* - *V* in Table 1). For each trajectory (containing 20,000 frames) the mean R_{PP} value (shown by points in Fig. 8) and the respective RMSD value of the constrained distances during the simulation (indicated by horizontal bars in Fig. 8) were calculated. For large time intervals, the appearance of water wire between phosphate groups obeys the Poisson distribution $P_t(k) = \frac{(\lambda t)^k}{k!}e^{-\lambda t}$, where λ is the probability that the event occurs *k* times in a time *t*. For each constrained distance R_{PP}, the maximum likelihood of the parameter of the Poisson distribution, λ (points in Fig. 8), and the 95% confidence intervals (vertical bars in Fig. 8) were calculated by the function "poissfit" of MatLab.

$\sigma_{POPC} = 1.5 \times 10^{14}\,cm^{-2}$ [13,56] and the total concentration of free proton in solution $6 \times 10^{20-(pH)}(cm^{-3})$, the one-way proton flux across the membrane over a unit area $S = 1\,cm^2$ per unit time $\Delta t = 1$ s reads

$$J_H = \frac{\Delta N}{\Delta t \cdot S} = k_{PT} \cdot 10^{pK_a - pH} \cdot \sigma_{POPC} = 12.6 \times 10^{14-pH}\ (cm^{-2}s^{-1}). \quad (10)$$

here ΔN is the amount of protons crossing the membrane in one direction in time Δt and S is the area of the membrane.

Generally the proton flux is proportional to the absolute concentration of free proton [H$^+$] near the membrane surface, whereas the resulting total flux is proportional to the proton concentration difference Δ[H$^+$]. Still in experiments, where the non-equilibrium pH shift is small (2.3ΔpH < < 1), Eq. (4) is fulfilled and the proton flux is proportional to ΔpH. Under these conditions, the proton flux J_H across the membrane (Eq. (10)) and the characteristic time τ_H of proton relaxation (Eq. (6)) both depend on pH. Nonetheless the proton permeability of membrane P_H, which relates these two characteristics (cf. Eqs. (3) and (6)), is a pH-independent parameter.

The estimations of P_H from MD simulations, as summarized in Fig. 8, give the value:.

$$P_H = J_H/[H^+] = 2.1 \times 10^{-6}\ cm\ s^{-1} \quad (11)$$

The obtained value of P_H is within the proton permeability range of 10^{-4}–10^{-8} cm s^{-1}, as measured with different lipid bilayers [7–21].

3.4. Tracing water in the hydrophobic membrane phase

We analyzed our MD simulation data to trace the presence of unsupported water clusters in the hydrophobic part of the membrane (the systems *B*, *C* were inspected, see Table 1). The membrane was divided into layers of 0.1 nm thickness in the *xy*-plane. The average amount of water clusters in each layer was calculated for the whole equilibrium trajectory. The black dashed lines in Fig. 9 show the distributions of phosphate groups from both sides of the membrane. The blue line in Fig. 9 shows the free energy of lone water molecules along the membrane normal.

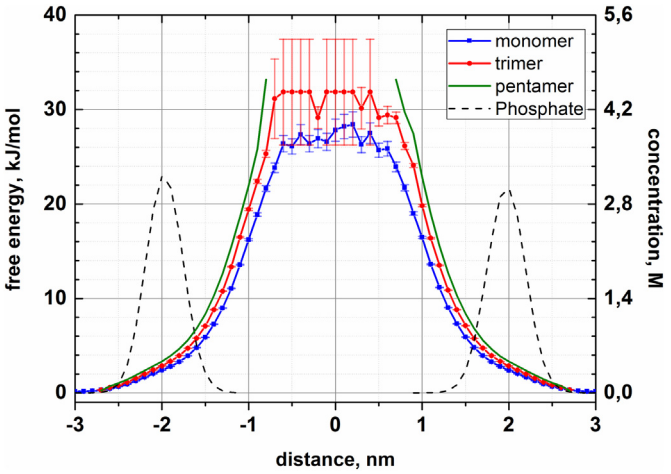

Fig. 9. Free energy profiles of water clusters inside the membrane as inferred from the MD simulation (the systems *B*, *C* of Table 1 were inspected). The free energy profile for lone water molecules is colored blue, water aggregates are shown by lines of different color (left axis). Dashed lines show, for comparison, the concentration of phosphate groups at the membrane/water interface (right axis). The water clusters were cued as *n*-connected graphs of *n* hydrogen-bonded water molecules by using a home-made MatLab script, the free energy was set to zero in the bulk. The vertical bars show the 95% confidence intervals for the free energy profiles of single water molecules (blue) and the water trimer (red) within the lipid bilayer. The probability W_n to find water cluster of the size *n* in the 95% confidence intervals (vertical bars in Fig. 9) were calculated by the function "poissfit" of MatLab using the productive equilibrium trajectory *C* (Table 1).

The free energy was calculated as $\Delta G(z_i) = -RT \cdot \ln \rho(z_i) + \Delta G_0$, where $\rho(z_i)$ is the water density in the layer z_i, and ΔG_0 was defined by setting the ΔG value in the bulk to zero. The energy penalty ΔG_1 for the transfer of a single water molecule from the bulk into the hydrophobic part of membrane was approx. +27 kJ/mol (Fig. 9), in exact agreement with the experimental value for transferring water into alkanes [83] and previous calculations [84]. We also looked for water clusters in the lipid bilayer (defined as aggregates of water molecules with intermolecular distances < 0.4 nm). The inspection of the MD simulation trajectories revealed one water trimer in the hydrophobic part of the bilayer, its energy profile is shown by the red line in Fig. 9. Water dimers, as well as tetramers and larger water clusters were observed only in the polar part of bilayer but not in its hydrophobic part (the energy distribution for a water pentamer is shown in Fig. 9 by a green solid line as an example).

Determination of energy profiles for single water molecules and a water trimer (Fig. 9) enabled the estimation of the free energy of a hydrogen bond (HB) in the hydrophobic phase. Indeed, provided that each water molecule forms, on average, 3.6 hydrogen bonds (HBs) in liquid water at room temperature [85], the transfer of a water molecule from the bulk into the hydrophobic phase would be accompanied by loss of approx. 1.8 HBs (since the former HB-partners of the water molecule would form HBs with each other), which would correspond to the free energy penalty (ΔG_{pen}) of +27 kJ/mol in Fig. 9. Transferring of three water molecules from the bulk into the hydrophobic phase would accordingly cost 3 × 27 kJ/mol = 81 kJ/mol. From the data in Fig. 9, the ΔG_{pen} value for bringing a water trimer in the hydrophobic phase

can be estimated as approx. +34 kJ/mol. Comparison of these values yields an estimate of approx. −47 kJ/mol for the three HBs of the water trimer. The free energy of a single HB in the hydrophobic phase could then be estimated as approx. −16 kJ/mol per bond, in agreement with the calculated free energies of HBs between water molecules in the gas phase [86,87]. In this framework, the ΔG_{pen} value for bringing a water trimer into the hydrophobic phase is smaller than the penalty for dimers, tetramers and pentamers of water (that could be estimated as approx. +38 kJ/mol, +45 kJ/mol and +56 kJ/mol, respectively), which may explain the absence of water dimers, tetramers or pentamers in the hydrophobic phase during the MD simulations (Fig. 9). The ΔG_{pen} value for a linear chain of n unsupported water molecules in the hydrophobic phase could be then estimated as $27 + (n\text{-}1) \times 11$ kJ/mol. Indeed, the addition of each water molecule to the chain will bring an energy penalty of losing 1.8 HBs in the bulk water (+27 kJ/mol) and a gain of one new HB in the hydrophobic phase (−16 kJ/mol). Accordingly, the presence of unsupported, stretched water chains with $n > 3$ is highly unlikely in the hydrophobic phase.

4. Discussion

4.1. Proton transfer via phospholipid-supported water wires

Here we combined experiments, steered MD simulations, and kinetic modelling to analyze the possibility of proton transfer between phospholipids of different membrane leaflets. Our MD simulations enabled extensive sampling of system conformations and, specifically, provided details of water structure near the oxygen atoms of ester linkers. We have found that converging of two lipid phosphate groups is coupled with arranging of oxygen atoms of their ester linkages into "oxygen passages" and aligning of water molecules along them.

The ability of confined water wires to conduct protons was predicted from theoretical considerations [7,14,43] and also shown experimentally in different systems [40,55,77,79,88]. The most recent calculation of Parrinello and colleagues showed that protons are transferred through transiently formed water wires even in the bulk water [55,89,90]. Building on these data, we suggest that the observed water wires, which were supported by oxygen atoms of lipid ester linkers (Figs. 2, 5, S2a–g), could serve as conduits for proton transfer between the lipid phosphate groups. Proton transfer along a preexisting water wire was calculated to take < 1 ps [40,55,77,78,89–91], i.e. to proceed much faster than formation of oxygen passages (> 10 ns, see Figs. 2, 5, S2a–g). Hence, proton transfer across phospholipid bilayers—via short water wires—would be kinetically controlled by the formation of supporting polar templates made of oxygen atoms of lipid ester linkages.

The proton transfer between the first/last water molecule of the wire and the adjoining phosphate group is unlikely to be rate limiting. Recent infrared spectroscopy and pulsed-field gradient nuclear magnetic resonance studies of dense phosphoric acid/water solutions showed that excess protons were "virtually shared between the phosphate and water oxygens" (quoted from [59]). These experimental observations correspond to MS-EVB calculations that showed protons forming contact ion pairs with phosphate groups; the authors noted that the contact ion pair wells were deeper than the wells of the protonated phosphate states [51]. From such a delocalized position between the phosphate group and water, the proton, being driven by thermal fluctuations and structural diffusion, can promptly get into the chain of water molecules.

The obvious instability of unsupported water clusters in the lipid phase (Fig. 9) is in agreement with earlier MD simulations where water chains collapsed within picoseconds when they were manually inserted into the hydrophobic bilayer and MD simulations were run without constraints [45,52,92].

In our MD simulations (Figs. 2, 5, S2a–g and [75]), in contrast, water molecules willingly entered the hydrophobic membrane layer and joined into wires each time when an oxygen passage had formed. Apparently, oxygen atoms of ester linkers attracted and aligned water molecules by serving as additional hydrogen bond partners. In the previous section, the penalty for adding a water molecule to a water chain in the hydrophobic phase has been estimated as approx. +11 kJ/mol. Then already one additional HB with ester oxygen(s) should be sufficient to stabilize a water molecule in the hydrophobic phase, provided that the free energy of this HB were < −11 kJ/mol.

The supported water wires in the lipid bilayer, as described here, resemble in many respects water wires within membrane ion channels, proton-translocating cavities of energy-converting enzymes, and nanotubes made of boron nitride or carbon [38–40,78,91,93]. Specifically, the nanotubes were shown to fluctuate between completely water-filled and empty states because of the high energetic cost of fragmented hydrogen bonds in a nanotube [40]. By analogy, upon formation of a lipid-oxygen-supported water wire, the closing of a transmembrane water chain (see Figs. 2, 5, S2a–g and [75]) should lead to an additional stabilization, because the incorporation of the "last" water molecule would be accompanied by formation not of one, but of two HBs with the neighboring water molecules.

Therefore, one could even expect reciprocal stabilization of supported water chains and their oxygen templates: once formed, a stable chain of water molecules would counteract the thermal disruption of the template. Indeed, the life time of water chains (up to 20 ns, Fig. 7) was longer than the characteristic motion time of phospholipid molecules (2–5 ns, Figs. S6, S7), and largely exceeded the sub-nanosecond dynamics of lipid tails in the middle of the bilayer. It is noteworthy that the MD simulation routine could not fully account for the particular tightness of hydrogen bonds in the hydrophobic phase [40,78,91], so that, in real membranes, the stability of such water chains might be even higher than observed in silico. Thus, the water wires and their supporting oxygen templates appear to behave as self-sustaining systems.

The formation of such oxygen templates would not per se require protonation/deprotonation events, which may explain the previously reported enigmatic insensitivity of the proton transfer to the H_2O/D_2O substitution [12,14]. As discussed above in relation to Eq. (6) and (10), the proton permeability coefficient should be independent of pH, in accordance with experimental observations [7,10,12,14,16,20].

The membrane dipole potential builds up as a cumulative dipole moment of the ester linkages of phospholipids [36]. Therefore, the assembly of these linkages into oxygen passages can hardly be sensitive to the membrane dipole potential. Hence, our suggestion on the kinetic limitation of proton transfer by the specific positioning of lipid ester linkages may explain why proton leakage was shown to be independent of the membrane dipole potential [12].

The formation of polar templates should, however, depend on the overall sampling rate of different lipid conformations, in agreement with the remarkable dependence of the proton transfer rate on temperature and membrane fluidity [9,14,17].

According to our estimates, proton transfer across the bilayer should mostly take place at the R_{PP} distance of ~1.6 nm (Fig. 8). Bringing the phosphorus atoms of two lipid molecules so close to each other corresponds to the ΔG value of ~ 55–60 kJ mol^{-1} (see Figs. 2 and S3), which matches the measured value of 55 ± 3.0 kJ mol^{-1} for the E_a of proton transfer through POPC bilayers (Fig. 1b) and is compatible with the earlier estimates of E_a [9,13,16,18].

Classical MD simulations cannot capture the delocalized nature of protons; they also provide no information on proton transfer between water molecules. However, QM-based dynamics calculation on time scales of tens of nanoseconds are still computationally too expensive for quantitative implementation. In addition, the inclusion of quantum effects would not notably affect the outcome of our study because the rate of proton displacement along water wires at < 1 ps [40,55,77,78,89–91], should be by several orders of magnitude faster that the formation of oxygen passages at nanoseconds (Figs. 2, 5,

S2a–g), which, as we argue here, appears to limit the overall rate of transmembrane proton transfer.

The proton diffusion at the membrane surface takes microseconds [51,58,94]. Hence, it is slower than the water wire formation and decay. Therefore, we did not consider the processes of proton delivery to the formed water wire, but only the conditional probability to find the buried phosphate in the protonated state: $\sigma_{POP(H)C} = 10^{(pKa)-(pH)} \times \sigma_{POPC}$. In the case when the proton-donating phosphate group is protonated and the proton-accepting phosphate group is deprotonated, the proton hop occurs at picoseconds; otherwise, the wire breaks up without proton translocation (unproductively).

The pK_a of a phosphate group has no fixed value, but reflects the local conditions for the given system conformation. For a phosphate group in aqueous solution, this value is about 2.0. At the membrane/water interface, owing to the surface Gouy-Chapman potential, the effective pKa is about 4.0 [13,56]. For a lipid phosphate group (or of a respective proton-phosphate ion pair) (blue and red curves in Fig. 4), the free energy difference between protonated and deprotonated states is $2.3k_BT\cdot(pH\text{-}pK_a)$ at the ambient pH of the solution. At pH 6.5, this difference is 15 kJ/mol on the membrane surface (blue arrow in Fig. 4); within the membrane this difference decreases and reaches zero at approx. 1 nm from the membrane center (the cross point of blue and red curves in Fig. 4). Therefore, the effective pKa of a lipid phosphate group increases with its immersion into the nonpolar part of lipid bilayer (see the black line in Fig. 4). The full free energy of the system is then the sum of contributions arising from the insertion of protonated and anionic phosphate groups into the bilayer (blue and red curves in Fig. 4, respectively) and of the free energy of phosphate protonation at the water/membrane interface $2.3k_BT\cdot(pH\text{-}pKa^0)$:

$$\Delta G(z) = \Delta G_{PO[P^-]C}(z) + \Delta G_{PO[PH]C}(z) + 2.3k_BT(pH - pKa^0) \quad (12)$$

In the transition state (when the water wire could form, see the red arrow in Fig. 4), the effective pKa values of both phosphate groups match approximately each other and also the physiological pH, which is important for the high kinetic efficiency of proton exchange between the groups.

The here presented mechanism combines elements of earlier hypothetical models of proton permeation across lipid bilayer. As in the original model of Nichols and Deamer [7], the mechanism invokes water wires; however, in our model, the wires are short, do not cross the whole membrane and, in addition, are supported by polar lipid atoms. As in the fatty acid model of Gutknecht [46], protons enter the membrane being carried by protonated and electrically neutral "vehicles", but these are protonated lipid phosphate groups. As in the cluster contact model of Haines [48], proton goes between two chemically similar, but differently protonated moieties when they approach the midplain of the bilayer from the opposite sides; however, these are phospholipid molecules, and not ionized water clusters.

In sum, the here suggested mechanism of proton transfer via self-sustaining water wires, which connect phosphate groups and are supported by polar oxygen atoms of lipids, quantitatively reproduces experimentally determined properties of proton transfer across lipid bilayers [6–21].

4.2. Physiological implications and outlook

While mitochondrial proton leaks are responsible for the loss of up to half of cellular energy in humans, the penetration of protons across the lipid bilayer is believed to be responsible only for the minor part of the proton leakage in mitochondria [1,2]. The major part of physiological proton leakage was suggested to be mediated by proteins of the inner mitochondrial membrane [19]. The protein-mediated proton leaks, similarly to the proton leakage through the lipid bilayer, show high proton specificity, relative insensitivity to pH, and dependence of membrane fluidity [2,53]. As argued elsewhere [95], some of these similarities might be due to the involvement of supported water wires also in protein-mediated proton leaks. The wires could run both through proteins or along protein/lipid interfaces. Hence, the whole proton leakage across energy-converting membranes, which is responsible for up to 50% of energy losses in humans [2], might be mediated by water wires supported by polar atoms of lipids and proteins present in the hydrophobic part of the membrane.

As noted in the Introduction, the main tenor in the evolution of energy-converting membranes is the increase in their tightness [28–31]. It was found that extremophilic organisms, to increase the tightness of their membrane, usually (i) elevate the density of non-polar carbon atoms in the midplane of the bilayer (e.g. by using lipid chains with terminal bulky aromatic groups) and (ii) decrease the overall mobility of the midplane (e.g. by using bipolar lipids that span the whole membrane), see [48,96–98] for reviews. In the framework of the here suggested mechanism, a dense, nonpolar, and rigid membrane midplane would hamper the formation of oxygen passages and thereby decrease the proton leaks.

Archaeal membranes are, generally, less permeable to protons than bacterial membranes, which allows acidophilic archaea to survive even at pH about zero [98]. It is tempting to speculate that the higher tightness of archaeal membranes to protons might be partly due to the ether linkers of archaeal lipids. Unlike ester linkers of bacterial lipids, each ether linker contains only one oxygen atom. Therefore, to form an oxygen passage, archaeal lipids should come closer to each other than bacterial lipids and/or engage oxygen atoms of more than two lipid molecules. It is noteworthy that the ability to synthesize ether-linked lipids by using oxygen-dependent enzymes has independently developed, after the oxygenation of the atmosphere, in eukaryotes [99]. In humans, alkyl- and alkenylphospholipids, with fatty acid tails in the *sn*-1 position attached by ether bonds, make 20% of all lipids; their fraction is maximal in the hearth where it reaches 40%. Mammals contain even dialkylglycerophosphocholines, analogous to archaeal lipids in that both hydrophobic tails are attached by ether linkers. In humans, dialkylglycerophosphocholines were reported only in the hearth and spermatozoa [100], for which minimization of energy losses is particularly important. It appears that, in humans, the physiological demand to suppress proton leakage in a particular tissue inversely correlates with the averaged number of oxygen atoms that link hydrophobic tails with polar heads in the lipids of this tissue.

In the view of particularly fast proton exchange between water and phosphate groups [59,60], another way to decrease proton leakage would be to use lipids without phosphate groups. And indeed, thylakoid membranes of photosynthetic organisms, which maintain ΔpH throughout the night, contain large fractions of glycolipids and sulfolipids, which would decrease the probability of an encounter between two phospholipid molecules.

As a future task, it seems worthy to clarify whether the supported water wires could be responsible for the non-linear dependence of membrane permeability (to diverse cations including protons) on the membrane potential. The dramatic increase in permeability at high membrane potential [101,102] is of great physiological importance because it attenuates the production of reactive oxygen species and, generally, prevents membrane damage [103]. Theoretical calculations predicted that water chains could be stabilized by an electric field that is oriented along the chains [40,104]. Hence, the membrane potential may increase the life time of supported water structures within lipid bilayer, which would favor ion leaks, since any ions, to get across the membrane, require water intrusions into the hydrophobic phase for solvation. Figuring out these and other properties and functions of supported water chains in biological membranes remains a challenge for future studies.

5. Conclusions

We show that transmembrane water wires could be supported not

only by proteins, but also by polar atoms of phospholipids and, specifically, by oxygen atoms of ester linkers, which has been previously overlooked. Our calculations show that proton transfer between the phosphate groups of opposing lipid molecules via short, supported water wires should be characterized by activation energy of approx. 50–60 kJ/mol, as well as weak dependence on the H_2O/D_2O substitution, membrane dipole potential and pH, all these traits being in agreement with experimentally determined properties of proton leakage across phospholipid bilayers.

Conflict of interests

The authors of the manuscript “Phospholipids as mediators of membrane proton leakage” have no conflict of interests

Transparency document

The Transparency document associated with this article can be found, in online version.

Acknowledgements

We gratefully acknowledge helpful discussions with Drs Boris V. Chernyak, Michael Y. Galperin, Joachim Heberle, Gerhard Hummer, Elena A. Kotova, and Vladimir. P. Skulachev. This work was supported by the *Deutsche Forschungsgemeinschaft*, the German Academic Exchange Service (DAAD), the EvoCell Program of the Osnabrueck University, the Development Programme of the Lomonosov Moscow State University (supercomputers ‘Chebyshev’ and ‘Lomonosov’), the Russia Government contract (AAAA-A19-119012890064-7), and grants from the Russian Science Foundation (14-50-00029, analysis of the MD data; 14-14-00592, kinetic modelling; 17-14-01314 mechanism of proton leakage in mitochondria).

Author contributions

DAC and AYM designed the study. MEB and DAC performed the calculations. AVL and NV prepared the liposomes and measured the proton leakage. MEB, DAC, AVL, NV, KVS, HJS and AYM analyzed and interpreted the data. MEB, DAC, AVL, NV, HJS, KVS and AYM wrote the paper.

Appendix A. Supplementary data

Supplementary data to this article can be found online at https://doi.org/10.1016/j.bbabio.2019.03.001.

References

[1] A.A. Starkov, Protein-mediated energy-dissipating pathways in mitochondria, Chem. Biol. Interact. 163 (2006) 133–144.
[2] M. Jastroch, A.S. Divakaruni, S. Mookerjee, J.R. Treberg, M.D. Brand, Mitochondrial proton and electron leaks, Essays Biochem. 47 (2010) 53–67.
[3] P. Mitchell, Coupling of phosphorylation to electron and hydrogen transfer by a chemi-osmotic type of mechanism, Nature 191 (1961) 144–148.
[4] W.A. Cramer, D.B. Knaff, Energy Transduction in Biological Membranes: A Textbook of Bioenergetics, Springer-Verlag, 1990.
[5] V.P. Skulachev, Membrane Bioenergetics, Springer-Verlag, Berlin Heidelberg, 1988.
[6] P. Mitchell, J. Moyle, Acid-base titration across the membrane system of rat-liver mitochondria. Catalysis by uncouplers, Biochem. J. 104 (1967) 588–600.
[7] J.W. Nichols, D.W. Deamer, Net proton-hydroxyl permeability of large unilamellar liposomes measured by an acid-base titration technique, Proc. Natl. Acad. Sci. U. S. A. 77 (1980) 2038–2042.
[8] C.M. Biegel, J.M. Gould, Kinetics of hydrogen ion diffusion across phospholipid vesicle membranes, Biochemistry 20 (1981) 3474–3479.
[9] M. Rossignol, P. Thomas, C. Grignon, Proton permeability of liposomes from natural phospholipid mixtures, Biochim. Biophys. Acta 684 (1982) 195–199.
[10] D.S. Cafiso, W.L. Hubbell, Electrogenic H^+/OH^- movement across phospholipid vesicles measured by spin-labeled hydrophobic ions, Biophys. J. 44 (1983) 49–57.
[11] K. Elamrani, A. Blume, Effect of the lipid phase transition on the kinetics of H^+/OH^- diffusion across phosphatidic acid bilayers, Biochim. Biophys. Acta 727 (1983) 22–30.
[12] W.R. Perkins, D.S. Cafiso, An electrical and structural characterization of H^+/OH^- currents in phospholipid vesicles, Biochemistry 25 (1986) 2270–2276.
[13] S. Grzesiek, N.A. Dencher, Dependency of ΔpH-relaxation across vesicular membranes on the buffering power of bulk solutions and lipids, Biophys. J. 50 (1986) 265–276.
[14] D.W. Deamer, Proton permeation of lipid bilayers, J. Bioenerg. Biomembr. 19 (1987) 457–479.
[15] I. Ahmed, G. Krishnamoorthy, Enhancement of transmembrane proton conductivity of protonophores by membrane-permeant cations, Biochim. Biophys. Acta 1024 (1990) 298–306.
[16] J.L. van de Vossenberg, T. Ubbink-Kok, M.G. Elferink, A.J. Driessen, W.N. Konings, Ion permeability of the cytoplasmic membrane limits the maximum growth temperature of bacteria and archaea, Mol. Microbiol. 18 (1995) 925–932.
[17] S. Paula, A.G. Volkov, A.N. Van Hoek, T.H. Haines, D.W. Deamer, Permeation of protons, potassium ions, and small polar molecules through phospholipid bilayers as a function of membrane thickness, Biophys. J. 70 (1996) 339–348.
[18] A.J.M. Driessen, J.L.C.M. van de Vossenberg, W.N. Konings, Membrane composition and ion-permeability in extremophiles, FEMS Microbiol. Rev. 18 (1996) 139–148.
[19] P.S. Brookes, A.J. Hulbert, M.D. Brand, The proton permeability of liposomes made from mitochondrial inner membrane phospholipids: no effect of fatty acid composition, Biochim. Biophys. Acta 1330 (1997) 157–164.
[20] J.L. van de Vossenberg, A.J. Driessen, W.D. Grant, W.N. Konings, Lipid membranes from halophilic and alkali-halophilic archaea have a low H^+ and Na^+ permeability at high salt concentration, Extremophiles 3 (1999) 253–257.
[21] I. Krishnamoorthy, G. Krishnamoorthy, Probing the link between proton transport and water content in lipid membranes, J. Phys. Chem. B 105 (2001) 1484–1488.
[22] T.E. Decoursey, Voltage-gated proton channels and other proton transfer pathways, Physiol. Rev. 83 (2003) 475–579.
[23] H. Hauser, D. Oldani, M.C. Phillips, Mechanism of ion escape from phosphatidylcholine and phosphatidylserine single bilayer vesicles, Biochemistry 12 (1973) 4507–4517.
[24] W. Hilpert, B. Schink, P. Dimroth, Life by a new decarboxylation-dependent energy conservation mechanism with Na as coupling ion, EMBO J. 3 (1984) 1665–1670.
[25] V.P. Skulachev, Sodium bioenergetics, Trends Biochem. Sci. 9 (1984) 483–485.
[26] A.Y. Mulkidjanian, P. Dibrov, M.Y. Galperin, The past and present of sodium energetics: may the sodium-motive force be with you, Biochim. Biophys. Acta 1777 (2008) 985–992.
[27] A.Y. Mulkidjanian, M.Y. Galperin, K.S. Makarova, Y.I. Wolf, E.V. Koonin, Evolutionary primacy of sodium bioenergetics, Biol. Direct 3 (2008) 13.
[28] A.Y. Mulkidjanian, M.Y. Galperin, E.V. Koonin, Co-evolution of primordial membranes and membrane proteins, Trends Biochem. Sci. 34 (2009) 206–215.
[29] D.W. Deamer, The first living systems: a bioenergetic perspective, Microbiol. Mol. Biol. Rev. 61 (1997) 239–261.
[30] D.V. Dibrova, M.Y. Chudetsky, M.Y. Galperin, E.V. Koonin, A.Y. Mulkidjanian, The role of energy in the emergence of biology from chemistry, Orig. Life Evol. Biosph. 42 (2012) 459–468.
[31] D.V. Dibrova, M.Y. Galperin, E.V. Koonin, A.Y. Mulkidjanian, Ancient systems of sodium/potassium homeostasis as predecessors of membrane bioenergetics, Biochem. Mosc. 80 (2015) 495–516.
[32] P. Mitchell, Foundations of vectorial metabolism and osmochemistry, Biosci. Rep. 11 (1991) 297–344 (discussion 345-296).
[33] I.V. Khavrutskii, A.A. Gorfe, B. Lu, J.A. McCammon, Free energy for the permeation of Na^+ and Cl^- ions and their ion-pair through a zwitterionic dimyristoyl phosphatidylcholine lipid bilayer by umbrella integration with harmonic fourier beads, J. Am. Chem. Soc. 131 (2009) 1706–1716.
[34] I. Vorobyov, T.E. Olson, J.H. Kim, R.E. Koeppe 2nd, O.S. Andersen, T.W. Allen, Ion-induced defect permeation of lipid membranes, Biophys. J. 106 (2014) 586–597.
[35] B.H. Honig, W.L. Hubbell, R.F. Flewelling, Electrostatic interactions in membranes and proteins, Annu. Rev. Biophys. Biophys. Chem. 15 (1986) 163–193.
[36] R.F. Flewelling, W.L. Hubbell, The membrane dipole potential in a total membrane potential model. Applications to hydrophobic ion interactions with membranes, Biophys. J. 49 (1986) 541–552.
[37] O.S. Andersen, A. Finkelstein, I. Katz, A. Cass, Effect of phloretin on the permeability of thin lipid membranes, J. Gen. Physiol. 67 (1976) 749–771.
[38] U. Ermler, G. Fritzsch, S.K. Buchanan, H. Michel, Structure of the photosynthetic reaction centre from Rhodobacter sphaeroides at 2.65 Å resolution: cofactors and protein-cofactor interactions, Structure 2 (1994) 925–936.
[39] Y. Zhou, J.H. Morais-Cabral, A. Kaufman, R. MacKinnon, Chemistry of ion coordination and hydration revealed by a K+ channel-Fab complex at 2.0 Å resolution, Nature 414 (2001) 43–48.
[40] J.C. Rasaiah, S. Garde, G. Hummer, Water in nonpolar confinement: from nanotubes to proteins and beyond, Annu. Rev. Phys. Chem. 59 (2008) 713–740.
[41] D.W. Deamer, J. Bramhall, Permeability of lipid bilayers to water and ionic solutes, Chem. Phys. Lipids 40 (1986) 167–188.
[42] S. Cukierman, E.P. Quigley, D.S. Crumrine, Proton conduction in gramicidin A and in its dioxolane-linked dimer in different lipid bilayers, Biophys. J. 73 (1997) 2489–2502.
[43] J.F. Nagle, Theory of passive proton conductance in lipid bilayers, J. Bioenerg. Biomembr. 19 (1987) 413–426.
[44] W. Shinoda, Permeability across lipid membranes, Biochim. Biophys. Acta 1858 (2016) 2254–2265.

[45] S.J. Marrink, F. Jahnig, H.J. Berendsen, Proton transport across transient single-file water pores in a lipid membrane studied by molecular dynamics simulations, Biophys. J. 71 (1996) 632–647.
[46] J. Gutknecht, Proton/hydroxide conductance and permeability through phospholipid bilayer membranes, Proc. Natl. Acad. Sci. U. S. A. 84 (1987) 6443–6446.
[47] A. Andreyev, T.O. Bondareva, V.I. Dedukhova, E.N. Mokhova, V.P. Skulachev, N.I. Volkov, Carboxyatractylate inhibits the uncoupling effect of free fatty acids, FEBS Lett. 226 (1988) 265–269.
[48] T.H. Haines, Do sterols reduce proton and sodium leaks through lipid bilayers? Prog. Lipid Res. 40 (2001) 299–324.
[49] H.L. Tepper, G.A. Voth, Protons may leak through pure lipid bilayers via a concerted mechanism, Biophys. J. 88 (2005) 3095–3108.
[50] A. Warshel, S.T. Russell, Calculations of electrostatic interactions in biological systems and in solutions, Q. Rev. Biophys. 17 (1984) 283–422.
[51] T. Yamashita, G.A. Voth, Properties of hydrated excess protons near phospholipid bilayers, J. Phys. Chem. B 114 (2010) 592–603.
[52] H.L. Tepper, G.A. Voth, Mechanisms of passive ion permeation through lipid bilayers: insights from simulations, J. Phys. Chem. B 110 (2006) 21327–21337.
[53] G.C. Brown, M.D. Brand, On the nature of the mitochondrial proton leak, Biochim. Biophys. Acta 1059 (1991) 55–62.
[54] G.A. Voth, Computer simulation of proton solvation and transport in aqueous and biomolecular systems, Acc. Chem. Res. 39 (2006) 143–150.
[55] N. Agmon, H.J. Bakker, R.K. Campen, R.H. Henchman, P. Pohl, S. Roke, M. Thamer, A. Hassanali, Protons and hydroxide ions in aqueous systems, Chem. Rev. 116 (2016) 7642–7672.
[56] Y. Zhou, R.M. Raphael, Solution pH alters mechanical and electrical properties of phosphatidylcholine membranes: relation between interfacial electrostatics, intramembrane potential, and bending elasticity, Biophys. J. 92 (2007) 2451–2462.
[57] A.A. Gurtovenko, J. Anwar, I. Vattulainen, Defect-mediated trafficking across cell membranes: insights from in silico modeling, Chem. Rev. 110 (2010) 6077–6103.
[58] A.Y. Mulkidjanian, J. Heberle, D.A. Cherepanov, Protons @ interfaces: implications for biological energy conversion, Biochim. Biophys. Acta 1757 (2006) 913–930.
[59] J.P. Melchior, K.D. Kreuer, J. Maier, Proton conduction mechanisms in the phosphoric acid-water system ($H_4P_2O_7$-H_3PO_4_2H_2O): a ^1H, ^{31}P and ^{17}O PFG-NMR and conductivity study, Phys. Chem. Chem. Phys. 19 (2016) 587–600.
[60] L. Vilciauskas, M.E. Tuckerman, G. Bester, S.J. Paddison, K.D. Kreuer, The mechanism of proton conduction in phosphoric acid, Nat. Chem. 4 (2012) 461–466.
[61] W.F. Bennett, D.P. Tieleman, Water defect and pore formation in atomistic and coarse-grained lipid membranes: pushing the limits of coarse graining, J. Chem. Theory Comput. 7 (2011) 2981–2988.
[62] M.G. Elferink, J.G. de Wit, A.J. Driessen, W.N. Konings, Stability and proton-permeability of liposomes composed of archaeal tetraether lipids, Biochim. Biophys. Acta 1193 (1994) 247–254.
[63] S. Pronk, S. Pall, R. Schulz, P. Larsson, P. Bjelkmar, R. Apostolov, M.R. Shirts, J.C. Smith, P.M. Kasson, D. van der Spoel, B. Hess, E. Lindahl, GROMACS 4.5: a high-throughput and highly parallel open source molecular simulation toolkit, Bioinformatics 29 (2013) 845–854.
[64] M. Parrinello, A. Rahman, Polymorphic transitions in single-crystals - a new molecular-dynamics method, J. Appl. Phys. 52 (1981) 7182–7190.
[65] W.G. Hoover, Canonical dynamics - equilibrium phase-space distributions, Phys. Rev. A 31 (1985) 1695–1697.
[66] S. Nose, A molecular-dynamics method for simulations in the canonical ensemble, Mol. Phys. 52 (1984) 255–268.
[67] B. Hess, P-LINCS: a parallel linear constraint solver for molecular simulation, J. Chem. Theory Comput. 4 (2008) 116–122.
[68] U. Essmann, L. Perera, M.L. Berkowitz, T. Darden, H. Lee, L.G. Pedersen, A smooth particle mesh Ewald method, J. Chem. Phys. 103 (1995) 8577–8593.
[69] S. Jo, T. Kim, V.G. Iyer, W. Im, CHARMM-GUI: a web-based graphical user interface for CHARMM, J. Comput. Chem. 29 (2008) 1859–1865.
[70] J.B. Klauda, R.M. Venable, J.A. Freites, J.W. O'Connor, D.J. Tobias, C. Mondragon-Ramirez, I. Vorobyov, A.D. MacKerell Jr., R.W. Pastor, Update of the CHARMM all-atom additive force field for lipids: validation on six lipid types, J. Phys. Chem. B 114 (2010) 7830–7843.
[71] W.L. Jorgensen, J. Chandrasekhar, J.D. Madura, R.W. Impey, M.L. Klein, Comparison of simple potential functions for simulating liquid water, J. Chem. Phys. 79 (1983) 926–935.
[72] G.N. Patey, J.P. Valleau, Free-energy of spheres with dipoles - Monte-Carlo with multistage sampling, Chem. Phys. Lett. 21 (1973) 297–300.
[73] G.M. Torrie, J.P. Valleau, Non-physical sampling distributions in Monte-Carlo free-energy estimation - umbrella sampling, J. Comput. Phys. 23 (1977) 187–199.
[74] W. Humphrey, A. Dalke, K. Schulten, VMD: visual molecular dynamics, J. Mol. Graph. 14 (1996) 33–38 (27-38).
[75] M.E. Bozdaganyan, A.V. Lokhmatikov, N. Voskoboynikova, D.A. Cherepanov, H.-J. Steinhoff, K.V. Shaitan, A.Y. Mulkidjanian, Aligning of water molecules into proton-conducting transmembrane water wires by oxygen atoms of phospholipid ester linkers (mediafile), (2019), https://doi.org/10.5281/zenodo.2613671.
[76] R. Pomes, B. Roux, Molecular mechanism of H^+ conduction in the single-file water chain of the gramicidin channel, Biophys. J. 82 (2002) 2304–2316.
[77] D.J. Mann, M.D. Halls, Water alignment and proton conduction inside carbon nanotubes, Phys. Rev. Lett. 90 (2003) 195503.
[78] V.R. Kaila, G. Hummer, Energetics and dynamics of proton transfer reactions along short water wires, Phys. Chem. Chem. Phys. 13 (2011) 13207–13215.
[79] R.H. Tunuguntla, F.I. Allen, K. Kim, A. Belliveau, A. Noy, Ultrafast proton transport in sub-1-nm diameter carbon nanotube porins, Nat. Nanotechnol. 11 (2016) 639–644.
[80] T. Grotthus, Mémoire sur la décomposition de l'eau et des corps qu'elle tient en dissolution à l'aide de l'électricité galvanique, Rome (1805).
[81] M. Akeson, D.W. Deamer, Proton conductance by the gramicidin water wire. Model for proton conductance in the F_1F_O ATPases? Biophys. J. 60 (1991) 101–109.
[82] D. Marx, A. Chandra, M.E. Tuckerman, Aqueous basic solutions: hydroxide solvation, structural diffusion, and comparison to the hydrated proton, Chem. Rev. 110 (2010) 2174–2216.
[83] P. Schatzberg, Solubilities of water in several normal alkanes from C_7 to C_{16}, J. Phys. Chem. 67 (1963) 776.
[84] K. Shinoda, W. Shinoda, M. Mikami, Efficient free energy calculation of water across lipid membranes, J. Comput. Chem. 29 (2008) 1912–1918.
[85] C.J. Sahle, C. Sternemann, C. Schmidt, S. Lehtola, S. Jahn, L. Simonelli, S. Huotari, M. Hakala, T. Pylkkanen, A. Nyrow, K. Mende, M. Tolan, K. Hamalainen, M. Wilke, Microscopic structure of water at elevated pressures and temperatures, Proc. Natl. Acad. Sci. U. S. A. 110 (2013) 6301–6306.
[86] F.N. Keutsch, J.D. Cruzan, R.J. Saykally, The water trimer, Chem. Rev. 103 (2003) 2533–2577.
[87] B.E. Rocher-Casterline, L.C. Ch'ng, A.K. Mollner, H. Reisler, Communication: determination of the bond dissociation energy (D_0) of the water dimer, $(H_2O)_2$, by velocity map imaging, J. Chem. Phys. 134 (2011) 211101.
[88] C. Dellago, M.M. Naor, G. Hummer, Proton transport through water-filled carbon nanotubes, Phys. Rev. Lett. 90 (2003) 105902.
[89] M. Ceriotti, J. Cuny, M. Parrinello, D.E. Manolopoulos, Nuclear quantum effects and hydrogen bond fluctuations in water, Proc. Natl. Acad. Sci. U. S. A. 110 (2013) 15591–15596.
[90] A. Hassanali, F. Giberti, J. Cuny, T.D. Kuhne, M. Parrinello, Proton transfer through the water gossamer, Proc. Natl. Acad. Sci. U. S. A. 110 (2013) 13723–13728.
[91] B.F. Habenicht, S.J. Paddison, M.E. Tuckerman, Ab initio molecular dynamics simulations investigating proton transfer in perfluorosulfonic acid functionalized carbon nanotubes, Phys. Chem. Chem. Phys. 12 (2010) 8728–8732.
[92] R.M. Venable, R.W. Pastor, Molecular dynamics simulations of water wires in a lipid bilayer and water/octane model systems, J.Chem.Phys. 116 (2002) 2663–2664.
[93] I.V. Khavrutskii, J.A. McCammon, Generalized gradient-augmented harmonic Fourier beads method with multiple atomic and/or center-of-mass positional restraints, J. Chem. Phys. 127 (2007) 124901.
[94] J. Heberle, J. Riesle, G. Thiedemann, D. Oesterhelt, N.A. Dencher, Proton migration along the membrane surface and retarded surface to bulk transfer, Nature 370 (1994) 379–382.
[95] A.Y. Mulkidjanian, D.N. Shalaeva, K.G. Lyamzaev, B.V. Chernyak, Does oxidation of mitochondrial cardiolipin trigger a chain of antiapoptotic reactions? Biochem. Mosc. 83 (2018) 1263–1278.
[96] W.N. Konings, S.V. Albers, S. Koning, A.J. Driessen, The cell membrane plays a crucial role in survival of bacteria and archaea in extreme environments, Antonie Van Leeuwenhoek 81 (2002) 61–72.
[97] W.N. Konings, Microbial transport: adaptations to natural environments, Antonie Van Leeuwenhoek 90 (2006) 325–342.
[98] M.F. Siliakus, J. van der Oost, S.W.M. Kengen, Adaptations of archaeal and bacterial membranes to variations in temperature, pH and pressure, Extremophiles 21 (2017) 651–670.
[99] H. Goldfine, The appearance, disappearance and reappearance of plasmalogens in evolution, Prog. Lipid Res. 49 (2010) 493–498.
[100] F. Snyder, T.-C. Lee, R.L. Wykle, Ether-linked lipids and their bioactive species, in: D.E. Vance, J.E. Vance (Eds.), Biochemistry of Lipids, Lipoproteins and Membranes, Elsevier, Amsterdam, 2002.
[101] G.C. Brown, M.D. Brand, Changes in permeability to protons and other cations at high proton motive force in rat liver mitochondria, Biochem. J. 234 (1986) 75–81.
[102] M.L. Garcia, M. Kitada, H.C. Eisenstein, T.A. Krulwich, Voltage-dependent proton fluxes in liposomes, Biochim. Biophys. Acta 766 (1984) 109–115.
[103] V.P. Skulachev, Uncoupling: new approaches to an old problem of bioenergetics, Biochim. Biophys. Acta 1363 (1998) 100–124.
[104] S. Vaitheeswaran, J.C. Rasaiah, G. Hummer, Electric field and temperature effects on water in the narrow nonpolar pores of carbon nanotubes, J. Chem. Phys. 121 (2004) 7955–7965.